Fast Identification of Volcanic Tremor and Lahar Signals during the 2009 Redoubt Eruption Using Permutation Entropy and Supervised Machine Learning

Kostas I. Konstantinou*[1], Diah Ayu Rahmalia[1], Izaina Nurfitriana[1,2], and Mie Ichihara[3]

Abstract

Despite their usefulness for volcano monitoring, emergent seismic signals, such as volcanic tremor or signals generated by lahars, are difficult to identify with confidence in a timely fashion. Machine-learning algorithms offer an objective alternative to traditional methods of identifying such volcanoseismic signals, because they are able to handle quickly large amounts of data, while requiring little input from the user. In this work, we combine permutation entropy and centroid as well as dominant frequency with supervised machine learning to evaluate their potential in identifying volcanic tremor and lahar signals recorded during the 2009 Redoubt volcano eruption. The particular dataset was chosen for the reason that the properties and occurrence times of the volcanoseismic signals during the eruption are well known from previous studies. We find that the selected features can effectively discriminate both types of signals against the seismic background, especially for stations that are near the source. Results show that the identification success rate for volcanic tremor reaches up to 96%, whereas this rate becomes up to 91% for lahar signals. The calculation of the features as well as the application of the machine-learning algorithms is fast, allowing their implementation in the operational environment of a volcano observatory during a volcanic crisis. Finally, the proposed methodology can potentially be used to objectively identify other emergent seismic signals such as tectonic tremor along subduction zones, glacial tremor, or seismic signals generated during landslides.

Cite this article as Konstantinou, K. I., D. Ayu Rahmalia, I. Nurfitriana, and M. Ichihara (2021). Fast Identification of Volcanic Tremor and Lahar Signals during the 2009 Redoubt Eruption Using Permutation Entropy and Supervised Machine Learning, *Seismol. Res. Lett.* **93**, 435–443, doi: 10.1785/0220210176.

Supplemental Material

Introduction

Seismological observations and their analyses are indispensable components of any volcano monitoring program, because early manifestations of magma ascent usually involve the occurrence of some form of seismic activity (Chouet and Matoza, 2013). Volcanoes can generate a variety of seismic signals ranging from earthquakes that are indistinguishable from common tectonic events to long-duration low-frequency signals that are more difficult to detect and analyze. The main difficulties posed by such signals are their emergent onset, the variability in their amplitude and duration (from seconds to hours or even days), as well as their frequency content that may partly overlap with seismic noise. Volcanic tremor is one example of such a signal that is generated along magma and/or fluid transporting conduits and is usually found to precede volcanic eruptions (Konstantinou and Schlindwein, 2003). Another example is seismic signals generated by lahars, which are catastrophic mud flows that move down the flank of volcanoes. From this description, it is obvious that both types of signals can be useful for volcano monitoring and as an early warning to catastrophic phenomena. However, any attempt to make use of them in near-real-time hinges upon the difficulty of confidently identifying each signal type in a timely fashion. In most cases, their recognition among the multitude of other seismic signals occurs in retrospect with the help of additional observations, for example, time-lapse cameras recording the lahar flow path. Hence, there is a need for developing

1. Department of Earth Sciences, National Central University, Taoyuan City, Taiwan, https://orcid.org/0000-0002-6290-9565 (KIK); 2. Geophysical Engineering Program, Institut Teknologi Sumatera, Lampung, Indonesia; 3. Earthquake Research Institute, The University of Tokyo, Tokyo, Japan

*Corresponding author: kkonst@cc.ncu.edu.tw

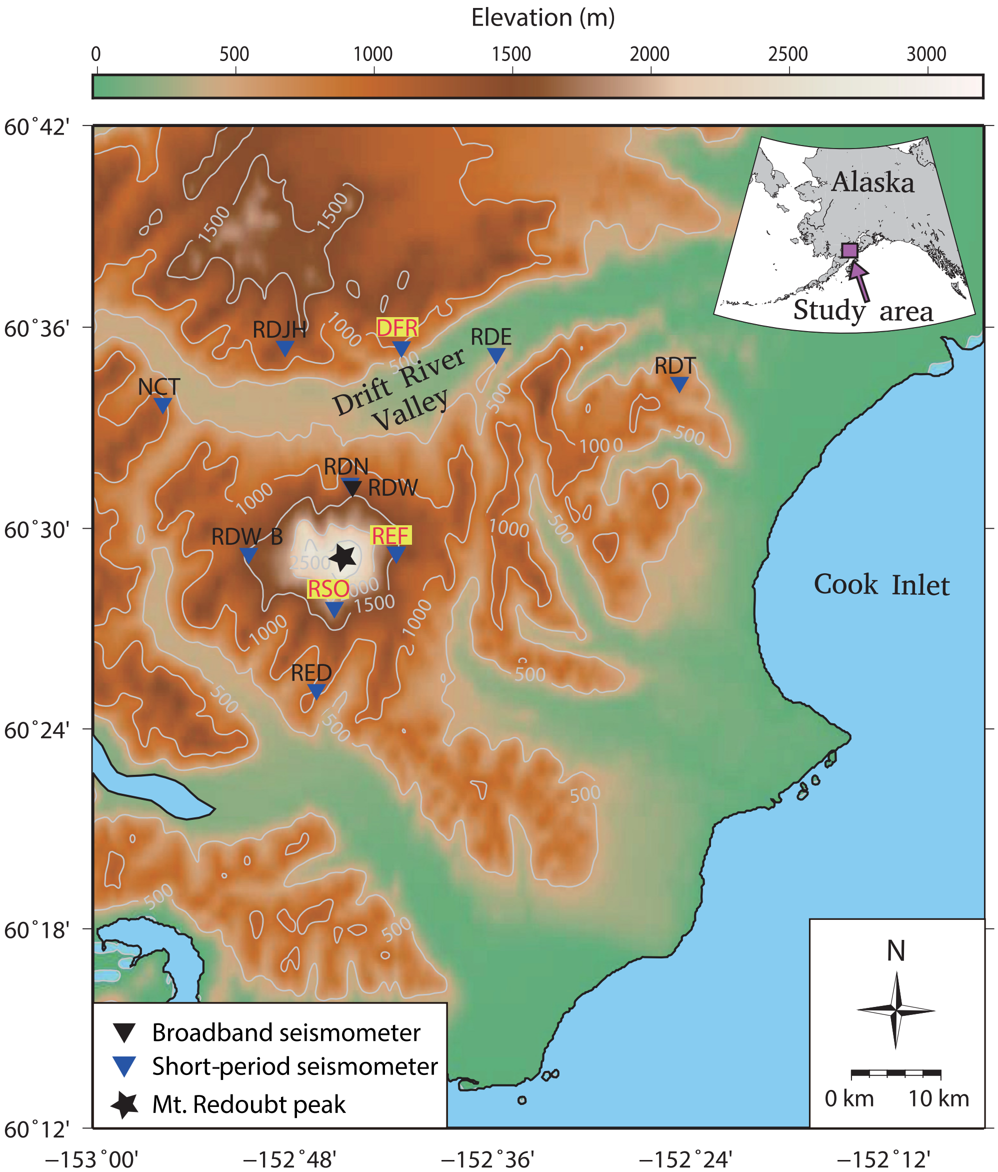

Figure 1. Map depicting the area around Redoubt volcano and the locations of the seismic stations that were recording continuous waveform data during the 2009 eruption. The inset in the upper right corner shows the location of the area relative to the map of Alaska. The seismic stations shown on the map are operated by the Alaska Volcano Observatory. The codes of stations used in this work are highlighted. The star indicates the eruptive vent during the 2009 eruption. The color version of this figure is available only in the electronic edition.

methodologies for the fast identification of these emergent signals within the operational setting of a volcano observatory.

During the last two decades, the quality and quantity of seismological observations at volcanoes have increased considerably, making manual analysis more cumbersome and at the same time less accurate. The term "machine learning" refers to a class of computer algorithms that improve their ability to perform tasks through training experience (Malfante *et al.*, 2018; Kong *et al.*, 2019). Machine-learning algorithms build a model based on sample data ("training dataset") for the purpose of applying this model to similar data ("testing dataset") that has not been used in the training process. In this context, one possible application of machine learning is the automatic recognition of a particular type of seismic signal when it occurs almost simultaneously with other signals. This is actually the situation that observatory staff faces during a volcanic crisis when the quantity of recorded data increases rapidly over a very short time span. A methodology that allows the fast recognition of volcanic tremor and lahar signals in an observatory setting should then fulfill two conditions: first, it should be able to handle a large volume of data, and, second, it should not critically depend on the subjective choice of parameters made by the user.

In this work, we evaluate the potential of automatically identifying tremor and lahar signals by combining machine-learning algorithms with features such as permutation entropy (PE) and spectral characteristics (centroid and dominant frequency). Continuous waveforms recorded during the 2009 eruption of Redoubt volcano in Alaska are utilized for this purpose, because Redoubt was sufficiently monitored at that time by the Alaska Volcano Observatory, and the seismic phenomena accompanying the eruption were well studied. We show that a combination of this small number of features with machine learning can be a fast and objective way to recognize such signals, and that the performance of our methodology is comparable to that of previously published studies that employed machine learning for volcanoseismic signal discrimination.

The 2009 Redoubt Eruption

Redoubt Volcano is a 3108 m high andesitic stratovolcano located in the west of the Cook Inlet, about 180 km southwest

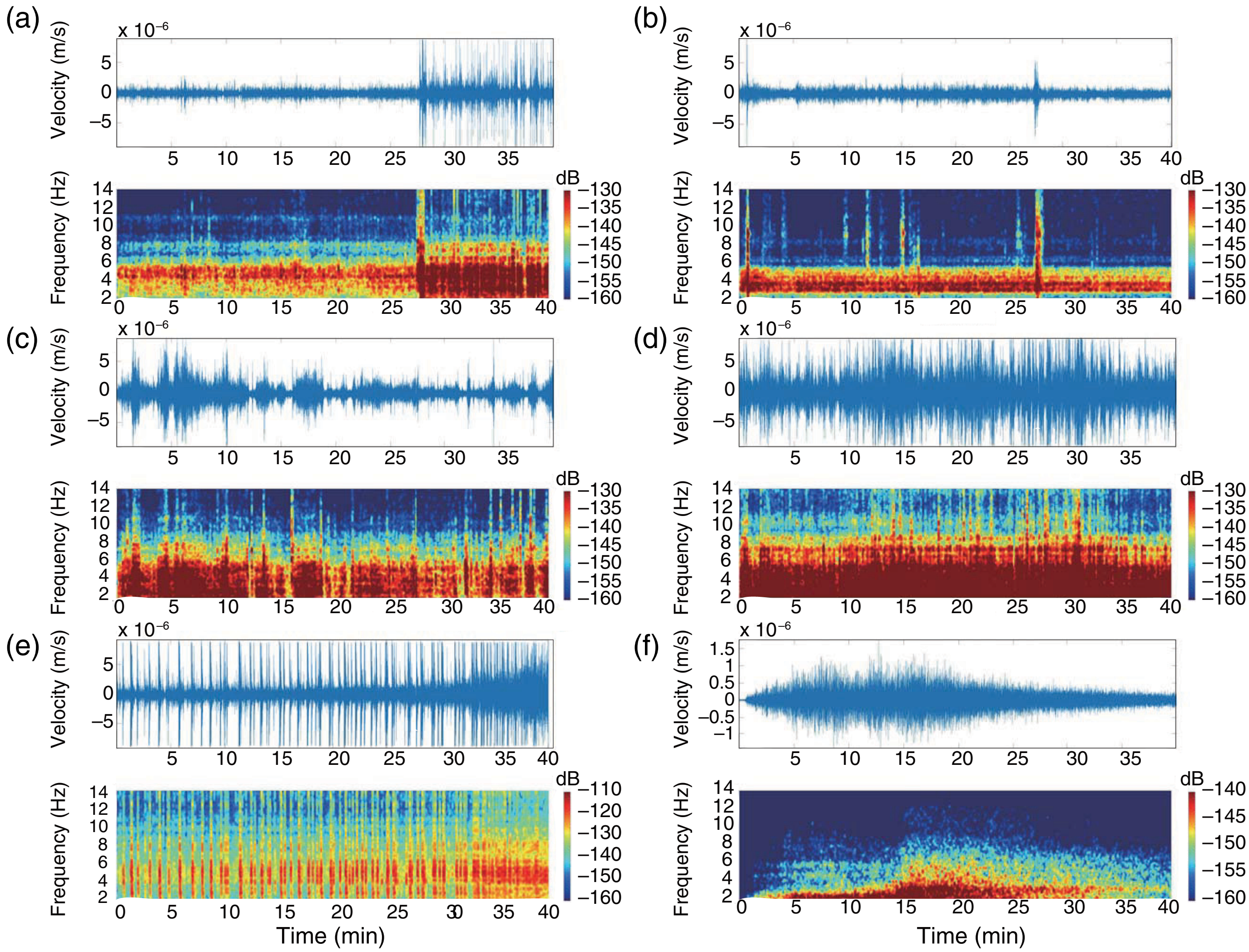

Figure 2. Unfiltered vertical-component waveforms and corresponding spectrograms for (a) high-amplitude precursory tremor that was recorded at station REF on 25 January 2009 10:20 UTC, (b) sustained precursory tremor that was recorded at station REF on 8 February 2009 12:00 UTC, (c) eruption tremor that was recorded at station RSO on 23 March 2009 22:00 UTC, (d) pseudoexplosion tremor recorded at station REF on 29 March 2009 22:30 UTC, (e) swarm tremor recorded at station REF on 27 March 2009 07:00 UTC, and (f) seismic signal generated by a lahar that was recorded at station DFR on 24 March 2009 03:00 UTC. The color version of this figure is available only in the electronic edition.

of Anchorage, Alaska (Fig. 1). After almost 20 yr of quiescence, Redoubt started showing signs of unrest, such as edifice deformation, in May 2008. At the time of the eruption, Redoubt was monitored by a local seismic network equipped with short-period sensors and one broadband seismometer (compare with Fig. 1). Bull and Buurman (2013) divided the course of events during the 2009 eruption into three phases, namely the precursory phase (July 2008–15 March 2009), the explosive phase (15 March–4 April 2009), and the effusive phase (4 April–1 July 2009). Except from deformation, the precursory phase was characterized by gas emissions, the occurrence of deep low-frequency earthquakes beneath the edifice, and by bursts of volcanic tremor during January and February 2009. The explosive phase consisted of a series of explosions that were followed by lava dome effusion, whereas seismic activity occurred in the form of earthquake swarms and bursts of volcanic tremor. Ice melting had already started taking place since early March, and the first lahar occurred 23 of the same month, to be followed by another 19 lahars until 4 April.

The volcanoseismic signals observed during the 2009 eruption of Redoubt have been described in terms of their temporal and spectral properties in a series of papers that were published in a special issue of *Journal of Volcanology and Geothermal Research* (for an overview, see Waythomas and Webley, 2013). Here, we only summarize the main characteristics of volcanic tremor and lahar signals, prompting the reader to refer to the papers contained in this special issue for more information. Examples of tremor and lahar waveforms along with their spectrograms can be seen in Figure 2. It should be noted that the terminology of the different tremor episodes shown in Figure 2 follows the one suggested by Buurman *et al.* (2013). Volcanic tremor exhibited large variations in amplitude and duration, containing energy at frequencies between 1 and 15 Hz, sometimes gliding to 20 Hz or higher (Hotovec *et al.*, 2013). These variations are probably a consequence of the different physical processes that might have been involved in its generation, such as degassing, boiling of the hydrothermal system, or extrusion of a lava dome (Buurman *et al.*, 2013; Hotovec *et al.*, 2013). On the other hand, the seismic signature of lahars is characterized by long duration (>10 min) and energy at frequencies up to 25 Hz (Buurman *et al.*, 2013).

Selected Features and Machine-Learning Algorithms

PE can be defined as a nonlinear statistical metric that quantifies complexity in a time series $x(t)$ by transforming it into vectors of delay L in an m-dimensional Euclidean space (i.e., $x(t), x(t+L), \ldots, x(t+(m-1)L)$ and then by partitioning the elements of these vectors into a sequence of symbols (Bandt and Pompe, 2002; Cao *et al.*, 2004; Staniek and Lehnertz, 2007). Formally, PE can be described as the Shannon entropy for k distinct symbols so that

$$H_p(m) = -\sum_{j=1}^{k} P_j \ln P_j, \tag{1}$$

in which P_j signifies the probability distribution of each distinct symbol (with $j = 1, 2, 3, \ldots, k$). To make the interpretation of the calculated values easier, $H_p(m)$ is usually normalized by dividing it with $\ln(m!)$, in which case PE will vary between 0 and 1, in which the former value signifies a purely deterministic signal and the latter indicates a purely stochastic one. This means that different signals will likely exhibit different ranges of PE—an attribute that can be exploited by machine-learning algorithms for automatically recognizing one signal type against all other. Continuous waveforms recorded at volcanoes have been previously used to calculate PE and study its temporal variations (Glynn and Konstantinou, 2016; Melchor *et al.*, 2020), which could also be utilized as a monitoring tool. Complementing PE as a feature for machine learning are two spectral characteristics, namely dominant and centroid frequency. The dominant frequency (f_d) of the signal is the frequency with the highest power in the calculated spectrum, whereas the centroid frequency (f_c) is defined as

$$f_c = \frac{\sum_{n=0}^{N-1} f(n)x(n)}{\sum_{n=0}^{N-1} x(n)}, \tag{2}$$

in which $f(n)$ is the center frequency of bin n, and $x(n)$ is its corresponding power value. The basic idea behind supervised machine learning is to deduce from training data a hyperplane decision surface that separates the different classes in an optimal way. Here, we use four such algorithms:

- Single-Layer Perceptron algorithm (Freund and Schapire, 1999) works by constructing a simple feedforward neural network and uses the Heaviside step function as the activation function.
- Sum of Errors Squared (SES) algorithm calculates iteratively the coefficients of the hyperplane decision surface $w^T x$ by minimizing the cost function:

$$J(w) = \sum_{i=1}^{N} (y_i - w^T x_i)^2, \tag{3}$$

  in which x_i are elements of the feature vector, and y_i is the class label of the training dataset.
- Multilayer Perceptron (MLP) algorithm uses a feedforward neural network along with a nonlinear activation function. MLP consists of at least three layers of nodes (i.e., input, hidden, and output layer). In this study, we utilized four hidden layers for tremor and 10 hidden layers for lahar signals, because these configurations exhibited the best performance.
- AdaBoost algorithm (Freund and Schapire, 1997) utilizes a large number of decision trees as "weak learners" that improve their classification results after each iteration. The trained algorithm is the weighted average of all these weak learners.

More details about the underlying theory and a full description of each algorithm can be found in Theodoridis and Koutroumbas (2009). Our choice of algorithms reflects a variable degree of sophistication and includes algorithms that thus far have not been used extensively in volcanoseismic studies. However, as already noted by Malfante *et al.* (2018), the choice of which machine-learning algorithm to use will not alter significantly the results as long as the selected features form a space where the different signals can be discriminated. A detailed description of the MATLAB functions used for these computations can be found in the supplemental material that accompanies this article.

Available Data and Feature Extraction

For the purposes of this study, we utilized continuous waveform data recorded by stations RSO, REF, DFR (compare with Fig. 1). RSO recorded volcanic tremor data with high fidelity owing to the fact that it was the closest station to the erupting vent, whereas DFR recorded the lahar-generated seismic signals owing to its location close to the lahars flow path. At this point, it should be noted that RSO was out of order from 23 March until 16 April, causing a significant gap in the recording of continuous data. This might seem as a good reason not to include this station in our analysis; however, outages of critical stations (owing to technical problems or eruption-related damage) are a rather common problem in volcano monitoring, and it would be interesting to see whether meaningful results can still be obtained in such cases. The remaining stations were either not available (RDE, RDW, RED), or owing to their location they did not record useful data within the study period (RDT, RDN, NCT, RDJH).

The continuous waveforms of the selected stations (sampled at 100 Hz) were split into 5 min nonoverlapping segments, and PE was calculated for each of these segments using embedding dimension $m = 5$ and delay time $L = 3$, as in previous applications of PE to seismological data (Glynn and Konstantinou, 2016; Melchor *et al.*, 2020). The condition for a reliable calculation of PE from observed time series is that the number of available samples is greater than $5m!$ (Bandt and Pompe, 2002). This means that more than $5 \times 5! = 600$ samples are needed, and, in our case, this condition is fulfilled because each segment contains 30,000 samples. Dominant and centroid frequencies (f_d, f_c) were also calculated for each segment, completing in this way the selected features that will be used as input to the machine-learning algorithms described earlier. Hereafter, we will refer to the triplet of values (PE, f_d, f_c) as an "event," in which each event then corresponds to a 5 min segment of continuous waveforms. All events were labeled as "volcanic tremor," "lahar signal," or "other" (i.e., any other signal including noise), based on the occurrence time of the different seismic phenomena during the eruption that were reported in Bull and Buurman (2013) and Buurman *et al.* (2013). The accuracy in the identification of the onset as well as end times for volcanic tremor and lahars ranges from 1 to 10 min; hence there is a possibility that some events were mislabeled. However, taking into account the time window we use for extracting features (5 min) and the fact that the duration of these signals is in the order of tens of minutes or even hours, we expect that this mislabeling affected only a small fraction of events. Plots of PE, centroid, and dominant frequency versus time at stations RSO, REF, and DFR can be found in Figures S1–S3.

We can gain some further insight into the nature of the data and the ability of the selected features to distinguish volcanic tremor and lahars signals from background seismicity by constructing histograms of PE, f_d, f_c for each station. Figures 3 and 4 show normalized histograms of these features for the three stations, more specifically RSO/REF for tremor and DFR for lahar signal recognition. To a large extent, PE can discriminate volcanic tremor from all other seismic signals at a nearby station such as RSO, but this discriminating power decreases at the more distant station REF. This can be easily explained in terms of seismic wave propagation through the heterogeneous structure of the volcano that produces smaller amplitudes and more scattering at high frequencies, eventually resulting in higher values of PE. The effect of distance from the vent can also be observed in the distribution of centroid frequency, with RSO exhibiting much less overlap than REF. On the other hand, dominant frequency seems to be much less affected by propagation effects at the different stations, owing to the fact that it attains values that are lower than 5 Hz. PE for the lahar signals exhibits good discriminating power at DFR, whereas the overlap between lahar and other signals is slightly more for centroid frequency. Dominant frequency also appears as a good discriminating feature at DFR exhibiting only small overlap. These observations can serve as a justification for the machine-learning approach adopted here, instead of opting for the apparently simpler approach of setting user-defined thresholds for the selected features. It is obvious that any choice of such thresholds would be highly subjective and would also have to be station dependent. This also implies that it may be quite risky to use training results obtained for a permanent station to identify signals at a temporary station installed after the eruption or crisis has begun.

Training and Cross Validation

We compiled 100 training and cross-validation datasets by randomly drawing events within the period from 1 January to 31 May 2009 under the constraint that events included in the training dataset are excluded from the cross-validation one. To avoid problems with unbalanced data, we set the proportion of tremor and lahar signals relative to other signals in each training dataset to be 60% and in each cross-validation dataset to be 40%. Six parameters are utilized to evaluate the performance of these algorithms, namely accuracy (A), precision (P), sensitivity (S), specificity (Sp), BER (balanced error), and bACC (balanced accuracy) score, which are defined as follows (Duque *et al.*, 2020; Lara-Cueva *et al.*, 2020):

$$\begin{aligned} A &= (N_C/N_T) \times 100\% \\ P &= [N_{\mathrm{TP}}/(N_{\mathrm{TP}} + N_{\mathrm{FP}})] \times 100\% \\ S &= [N_{\mathrm{TP}}/(N_{\mathrm{TP}} + N_{\mathrm{FN}})] \times 100\% \\ \mathrm{Sp} &= [N_{\mathrm{TN}}/(N_{\mathrm{TN}} + N_{\mathrm{FP}})] \times 100\% \\ \mathrm{BER} &= [1 - (S + \mathrm{Sp})/(2 \times 100)] \times 100\% \\ \mathrm{bACC} &= [(S + \mathrm{Sp})/2]\%, \end{aligned}$$

in which N_C is the number of correctly identified events, N_T is the total number of events in each dataset, N_{TP} is the number of true positives, N_{FN} is the number of false negatives, N_{TN} is the number of true negatives, and N_{FP} is the number of false positives. It should be noted that the BER score represents a measure of misidentified events in the sense that BER equal to 0.01 indicates that one out of 100 events is misidentified; hence the BER score should be as small as possible. On the contrary, the bACC score combines the sum of sensitivity and specificity divided by 2, which is the number of classes in the data that need to be separated (in our case we have class 1: tremor or lahar signals, class 2: all other signals including noise). For the results to be meaningful, bACC score should be as large as possible.

We first trained the four machine-learning algorithms using the 100 tremor and lahar training datasets and then applied them to the corresponding testing datasets, calculating for each one the values of the six performance parameters at each

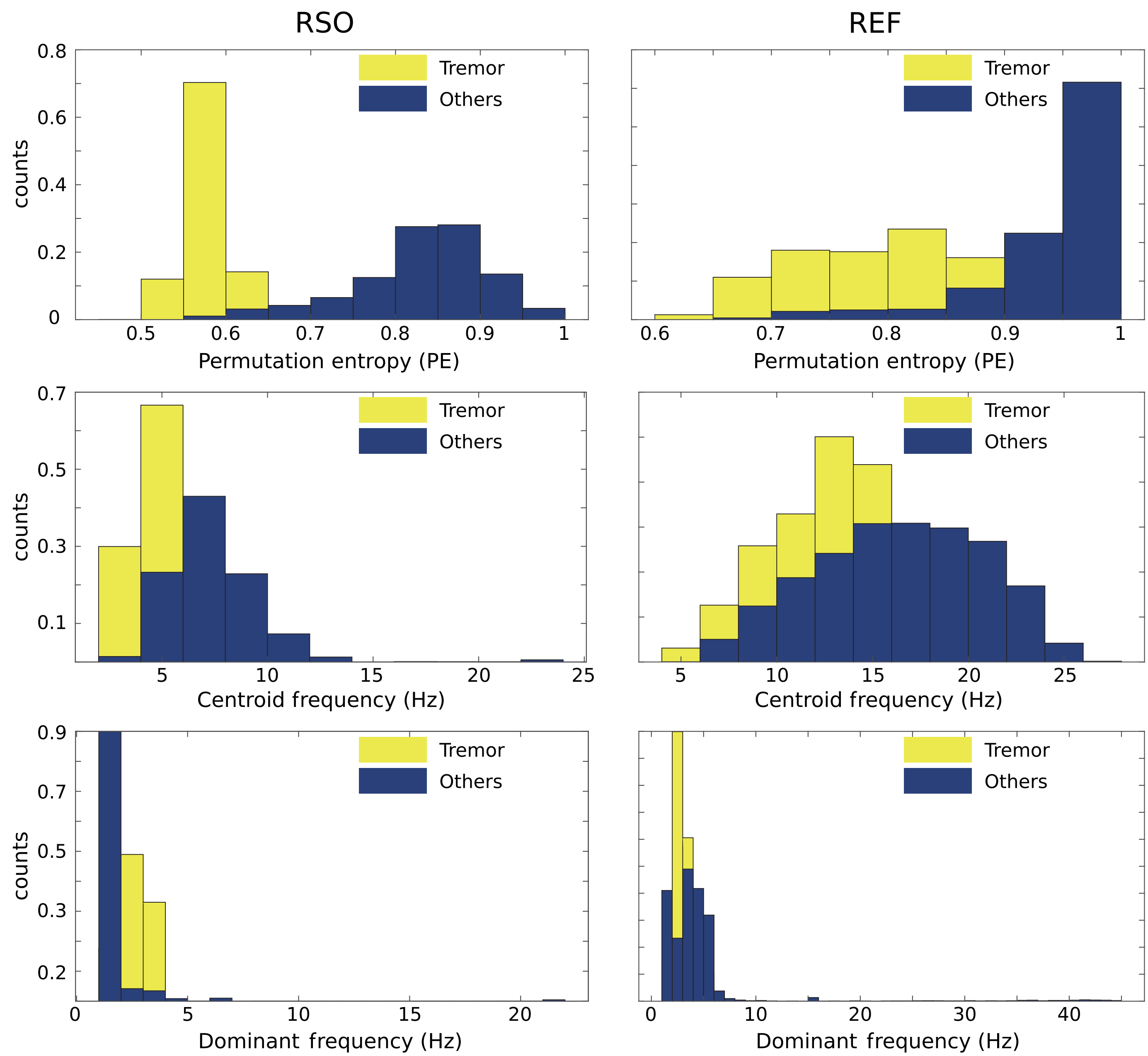

station. Figure 5 summarizes the performance parameters for the four algorithms by listing their mean values for volcanic tremor at stations RSO/REF and for lahar signals at station DFR. As it can be seen, station RSO exhibited the best results in tremor recognition with mean BER and bACC scores of 4%–5% and 95%–96%, respectively, whereas the standard errors were in the order of 1%. Station REF exhibited a worse performance (especially for MLP) with BER score between 15% and 23% and bACC score 77%–85% with MLP having a bACC score of 77%. These results suggest that the outage period of station RSO, significant as it was, influenced very little the performance of the algorithms and also underlines the importance of having stations near the erupting vent.

The situation for the lahar recognition performance is more complicated, mostly due to the smaller number of events corresponding to lahar signals in the training and testing datasets. The SES algorithm performed quite poorly with very low mean sensitivity (10%), high BER score (45%), and relatively low bACC score (55%). The other three algorithms exhibited much better performance with high bACC score (>80%) and acceptable BER score (9%–11%); however, the mean value of the precision parameter varies strongly (25%–83%) among them. In an effort to check whether these results depend on the embedding dimension used for PE calculation, we

Figure 3. Normalized histograms of the three features used in this study that compare the distribution of each feature for volcanic tremor and all other signals at stations RSO and REF. The color version of this figure is available only in the electronic edition.

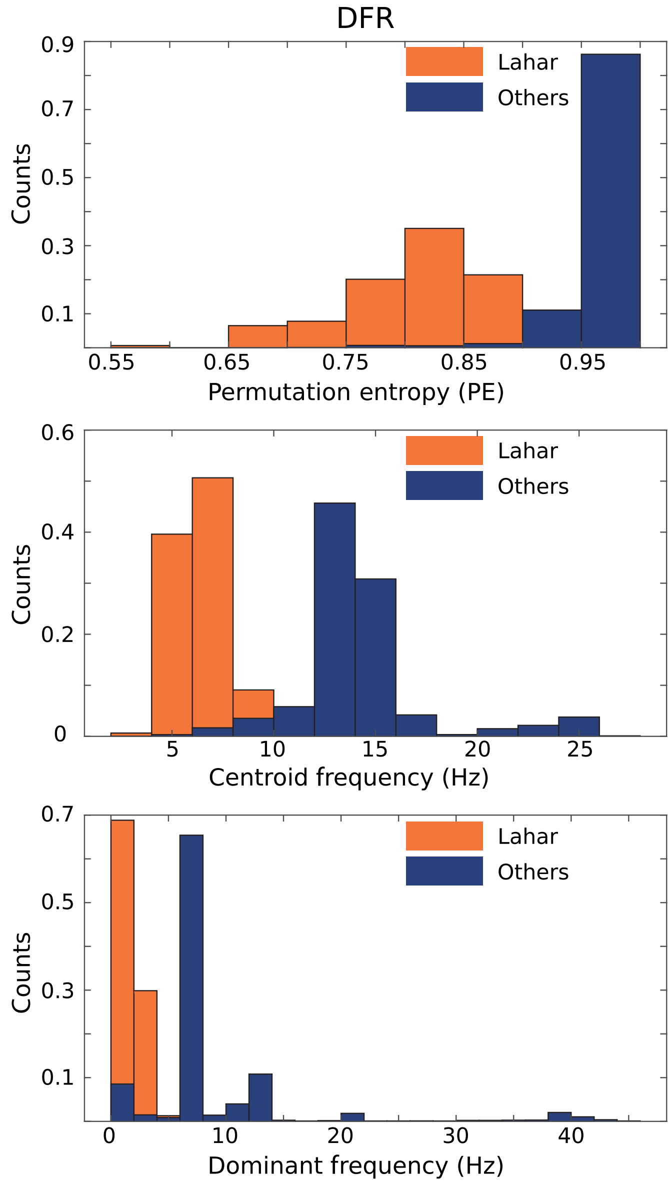

Figure 4. Normalized histograms of the three features used in this study that compare the distribution of each feature for lahar and all other signals at station DFR. The color version of this figure is available only in the electronic edition.

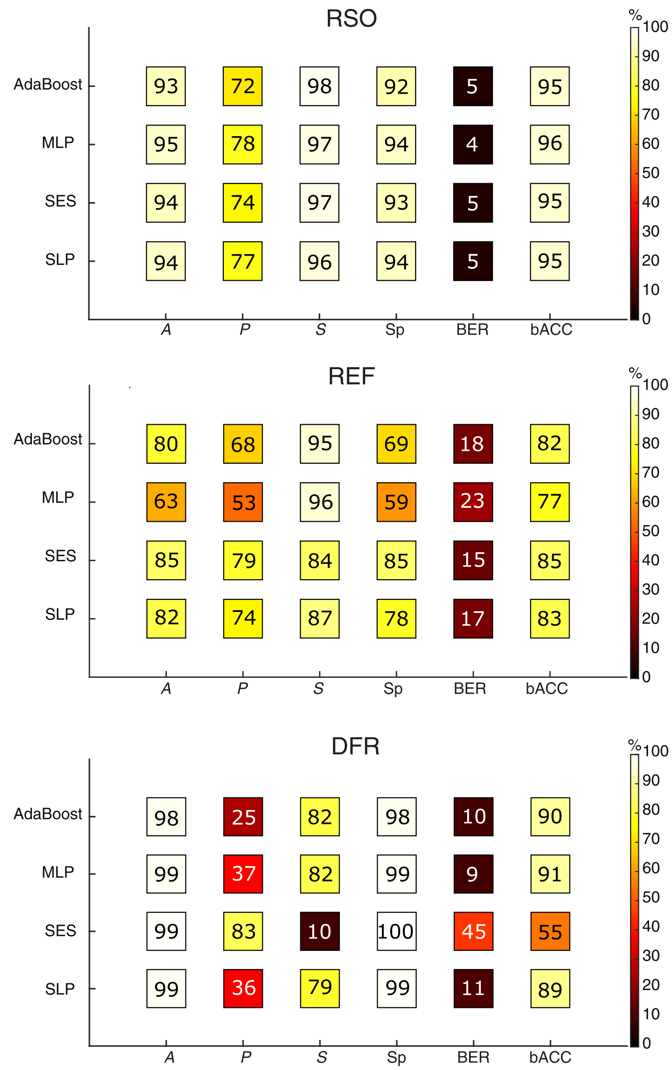

Figure 5. Graphical depiction of the performance parameters at each station for the different machine-learning algorithms used in this study. Each performance parameter box is shaded according to the scale at the right side of each panel. The number inside each box represents the mean value of each parameter for 100 randomized datasets used for cross validation. MLP, Multilayer Perceptron; SES, sum of errors squared; SLP, Single-layer Perceptron. The color version of this figure is available only in the electronic edition.

recalculated PE using different combinations of m and L ($m = 6$, $L = 3$; $m = 5$, $L = 2$; $m = 5$, $L = 4$) and repeated the training and testing in the same way as previously described. Figures S4–S6 give a graphical depiction of the performance parameters, indicating that changes in m and L in the calculation of PE have very little influence on our results (differences in the mean values of performance parameters are, in most cases, less than 10%). From the point of view of computer time, a typical run for datasets consisting of 8000–13,000 events on a PC with eight Intel i7-3770 cores using MATLAB R2018a, showed that the SES algorithm was the fastest (~0.31 s) followed by AdaBoost (~63 s).

Concluding Remarks

Most of the previous studies that utilized supervised machine learning for classifying volcanoseismic signals relied on a large number of extracted features (Maggi *et al.*, 2017; Malfante *et al.*, 2018; Ren *et al.*, 2020). This approach has a sound logical basis in the sense that increasing the number of features offers more discriminating power if many different types of signals need to be classified. However, a large number of features are redundant in cases when the goal is to simply identify a particular volcanoseismic signal against all other. In this study, we showed that this can be achieved using three such features in the case of volcanic tremor and lahar signals. The selected features (PE, f_d, f_c) were found to have good discriminating power with successful identification of 96 out of 100 events for tremor and 90 out of 100 events for lahar signals, whereas the results depended only weakly on the chosen machine-learning algorithm. More specifically, our results highlighted that the selected features can achieve high success rates in tremor identification even if a simple (but fast) algorithm such as SES is employed. Such an algorithm may perform poorly for lahar signals; however, in this case AdaBoost is a good alternative exhibiting the best trade-off between speed (∼63 s) and performance (compare with Fig. 5).

The methodology proposed in this work has a number of advantages that make it ideal for implementation in volcano observatories. First, only three parameters need to be specified by the user: namely, m, L for PE calculation, and window length. As shown previously, the results do not critically depend on the first two parameters, whereas the third one can be objectively determined based on the sampling rate of the data and the emergent nature of the signals that need to be identified. Second, the calculation of all features can be done relatively fast, and along with a suitable algorithm (SES or AdaBoost) identification results from one or more stations can be provided within a few minutes. Third, once the quantities PE, f_d, f_c are calculated, their temporal variation can further be utilized for monitoring purposes, as shown previously by Glynn and Konstantinou (2016) and Melchor *et al.* (2020). Finally, the proposed methodology could potentially be applied to other emergent (and difficult to detect) signals of geophysical interest. Such signals may include tectonic tremor along subduction zones, glacial tremor induced by ice melting, and seismic signals related to landslides.

Data and Resources

The continuous waveform data that were used in this study can be obtained from the Incorporated Research Institutions for Seismology (IRIS) Data Management Center (https://ds.iris.edu/ds/nodes/dmc). The MATLAB functions that implement the machine-learning algorithms employed in this work are freely available as an electronic supplement of Theodoridis and Koutroumbas (2009; https://booksite.elsevier.com/9780123744869). All websites were last accessed in June 2021. Supplemental material for this article includes a description of the computational procedure followed, three MATLAB functions that compute permutation entropy (PE) and spectral features (uploaded separately), as well as six figures showing the temporal variation of the selected features and machine-learning results for different values of m and L.

Declaration of Competing Interests

The authors declare no competing interests.

Acknowledgments

This research has been supported by the Ministry of Science and Technology of Taiwan (MOST) through a grant awarded to the first author. Diah Ayu Rahmalia and Izaina Nurfitriana have been supported by scholarships provided by National Central University and through the Sakura program of the Earthquake Research Institute, the University of Tokyo. The authors would like to thank Editor-in-Chief Alison Bent and the Associate Editor for handling this article, as well as Alicia Hotovec-Ellis and an anonymous reviewer for their constructive comments.

References

Bandt, C., and B. Pompe (2002). Permutation entropy: A natural complexity measure for time series, *Phys. Rev. Lett.* **88,** 174102.

Bull, K. F., and H. Buurman (2013). An overview of the 2009 eruption of Redoubt volcano, Alaska, *J. Volcanol. Geoth. Res.* **259,** 2–15, doi: 10.1016/j.jvolgeores.2012.06.024.

Buurman, H., M. E. West, and G. Thompson (2013). The seismicity of the 2009 Redoubt eruption, *J. Volcanol. Geoth. Res.* **259,** 16–30, doi: 10.1016/j.jvolgeores.2012.04.024.

Cao, Y., W. Tung, J. B. Gao, V. A. Protopopescu, and L. M. Hively (2004). Detecting dynamical changes in time series using the permutation entropy, *Phys. Rev. E* **70,** no. 4, doi: 10.1103/physreve.70.046217.

Chouet, B. A., and R. S. Matoza (2013). A multi-decadal view of seismic methods for detecting precursors of magma movement and eruption, *J. Volcanol. Geoth. Res.* **252,** 108–175, doi: 10.1016/j.jvolgeores.2012.11.013.

Duque, A., K. Gonzalez, N. Perez, D. Benitez, F. Grijalva, R. Lara-Cueva, and M. Ruiz (2020). Exploring the unsupervised classification of seismic events of Cotopaxi volcano, *J. Volcanol. Geoth. Res.* **403,** 107009, doi: 10.1016/j.jvolgeores.2020.107009.

Freund, Y., and R. E. Schapire (1997). A decision-theoretic generalization of on-line learning and an application to boosting, *J. Comput. Syst. Sci.* **55,** 119–139, doi: 10.1006/jcss.1997.1504.

Freund, Y., and R. E. Schapire (1999). Large margin classification using the perceptron algorithm, *Mach. Learn.* **37,** 277–296, doi: 10.1023/A:1007662407062.

Glynn, C. C., and K. I. Konstantinou (2016). Reduction of randomness in seismic noise as a short-term precursor to a volcanic eruption, *Sci. Rep.* **6,** 37733, 1–9, doi: 10.1038/srep37733.

Hotovec, A. J., S. G. Prejean, J. E. Vidale, and J. Gomberg (2013). Strongly gliding harmonic tremor during the 2009 eruption of Redoubt volcano, *J. Volcanol. Geoth. Res.* **259,** 89–99, doi: 10.1016/j.jvolgeores.2012.01.001.

Kong, Q., D. T. Trugman, Z. E. Ross, M. J. Bianco, B. J. Meade, and P. Gerstoft (2019). Machine learning in seismology: Turning data into insights, *Seismol. Res. Lett.* **90,** 3–14, doi: 10.1785/0220180259.

Konstantinou, K. I., and V. Schlindwein (2003). Nature, wavefield properties and source mechanism of volcanic tremor: A review, *J. Volcanol. Geoth. Res.* **119,** 161–187.

Lara-Cueva, R., J. C. Larco, D. S. Benitez, N. Perez, F. Grijalva, and M. Ruiz (2020). On finding possible frequencies for recognizing microearthquakes at Cotopaxi volcano, *J. Volcanol. Geoth. Res.* **407,** 107092, doi: 10.1016/j.jvolgeores.2020.107092.

Maggi, A., V. Ferrazzini, C. Hibert, F. Beauducel, P. Boissier, and A. Amemotou (2017). Implementation of a multistation approach for automated event classification at Piton de la Fournaise volcano, *Seismol. Res. Lett.* **88,** no. 3, 878–891, doi: 10.1785/0220160189.

Malfante, M., M. Dalla Mura, J.-P. Metaxian, J. I. Mars, O. Macedo, and A. Inza (2018). Machine learning for volcano-seismic signals, *IEEE Signal Process. Mag.* **35,** 1053–5888, doi: 10.1109/MSP.2017.2779166.

Melchor, I., J. Almendros, R. Carniel, K. I. Konstantinou, M. Hantusch, and A. Caselli (2020). On data reduction methods for volcanic tremor characterization: The 2012 eruption of Copahue volcano, Southern Andes, *Earth Planets Space* **72,** Article Number 134, doi: 10.1186/s40623-020-01270-7.

Ren, C. X., A. Peltier, V. Ferrazzini, B. Rouet-Leduc, P. A. Johnson, and F. Brenguier (2020). Machine learning reveals the seismic signature of eruptive behavior at Piton de la Fournaise volcano, *Geophys. Res. Lett.* **47,** e2019GL085523, doi: 10.1029/2019GL085523.

Staniek, M., and K. Lehnertz (2007). Parameter selection for permutation entropy measurements, *Int. J. Bifurcat. Chaos* **17,** no. 10, 3729–3733.

Theodoridis, S., and K. Koutroumbas (2009). *Pattern Recognition*, Academic Press, Oxford, United Kingdom.

Waythomas, C. F., and P. W. Webley (2013). Preface to the special issue of JVGR on the 2009 eruption of Redoubt volcano, Alaska, *J. Volcanol. Geoth. Res.* **259,** 1, doi: 10.1016/j.jvolgeores.2013.05.013.

Manuscript received 2 July 2021
Published online 17 November 2021